Non-Heme Manganese Catalysts for On-Demand Production of Chlorine Dioxide in Water and Under Mild Conditions

ARTICLE *in* JOURNAL OF THE AMERICAN CHEMICAL SOCIETY · FEBRUARY 2014

Impact Factor: 12.11 · DOI: 10.1021/ja5001642 · Source: PubMed

8 AUTHORS, INCLUDING:

Silei Xiong
Purdue University
10 PUBLICATIONS **35** CITATIONS
SEE PROFILE

Seungwoo Hong
Harvard University
19 PUBLICATIONS **404** CITATIONS
SEE PROFILE

Mahdi M Abu-Omar
Purdue University
147 PUBLICATIONS **4,074** CITATIONS
SEE PROFILE

JACS
JOURNAL OF THE AMERICAN CHEMICAL SOCIETY
Article
pubs.acs.org/JACS

Non-Heme Manganese Catalysts for On-Demand Production of Chlorine Dioxide in Water and Under Mild Conditions

Scott D. Hicks,[†] Doyeon Kim,[‡] Silei Xiong,[§] Grigori A. Medvedev,[§] James Caruthers,[§] Seungwoo Hong,[‡] Wonwoo Nam,*[,‡] and Mahdi M. Abu-Omar*[,§,†]

[†]Brown Laboratory, Negishi Brown Institute, and Department of Chemistry, Purdue University, 560 Oval Drive, West Lafayette, Indiana 47907, United States

[‡]Department of Bioinspired Science, Department of Chemistry and Nano Science, Ewha Womans University, Seoul 120-750, Korea

[§]School of Chemical Engineering, Purdue University, Forney Hall of Chemical Engineering, 480 Stadium Mall Drive, West Lafayette, Indiana 47907, United States

Supporting Information

ABSTRACT: Two non-heme manganese complexes are used in the catalytic formation of chlorine dioxide from chlorite under ambient temperature at pH 5.00. The catalysts afford up to 1000 turnovers per hour and remain highly active in subsequent additions of chlorite. Kinetic and spectroscopic studies revealed a $Mn^{III}(OH)$ species as the dominant form under catalytic conditions. A $Mn^{III}(\mu\text{-}O)Mn^{IV}$ dinuclear species was observed by EPR spectroscopy, supporting the involvement of a putative $Mn^{IV}(O)$ species. First-order kinetic dependence on the manganese catalyst precludes the dinuclear species as the active form of the catalyst. Quantitative kinetic modeling enabled the deduction of a mechanism that accounts for all experimental observations. The chlorine dioxide producing cycle involves formation of a putative $Mn^{IV}(O)$, which undergoes PCET (proton coupled electron-transfer) reaction with chlorite to afford chlorine dioxide. The ClO_2 product can be efficiently removed from the aqueous reaction mixture via purging with an inert gas, allowing for the preparation of pure chlorine dioxide for on-site use and further production of chlorine dioxide.

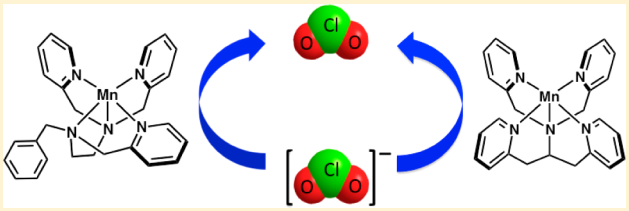

INTRODUCTION

The chlorine oxyanions (ClO_n^-, n = 1−4) spanning oxidation states of +1 to +7 have found diverse uses from bleaching agents to oxidizers in rocket fuels. As a result of their high solubility in water and wide range of applications, water sources have been severely contaminated by these toxic anthropogenic pollutants.[1] Perchlorate (ClO_4^-) is commonly used as an oxidant in rocket fuel, missiles, and fireworks.[2] Advances in perchlorate remediation with use of microbes[3] as well as chemical catalysts[4] have previously been discussed. Chlorate (ClO_3^-) is used as an herbicide and a source of chlorine dioxide (ClO_2). Chlorite (ClO_2^-) is primarily used as a source of ClO_2 in the pulp bleaching industry, and hypochlorite (ClO^-) is a widely used disinfectant. Of the aforementioned chlorine-containing species, the catalytic conversion of chlorite to either dioxygen and chloride or chlorine dioxide is of great interest. The reactivity of chlorite and chlorous acid, Cl^{III}, has been studied extensively.[5] The reactivity of aqua transition-metal ions toward Cl^{III} has been reviewed by Fábián.[6] Collman and Braumann have shown that metalloporphyrins catalyze the electrochemical reduction of chlorite[7] as well as alkane oxidations with chlorite as an oxidant.[8] The Environmental Protection Agency has recently labeled chlorite as a major water contaminant as a result of suspected health risks such as childhood anemia.[9] Chlorite can also serve as an oxidizing or chlorinating agent when exposed to water pollutants and consequently enhance toxicity. Therefore, a method to remediate chlorite is of interest from an environmental standpoint.

The biological remediation of ClO_4^- occurs in three steps catalyzed by two enzymes.[10] Perchlorate reductase is a molybdopterin-dependent enzyme proposed to catalyze the reduction of ClO_4^- to ClO_2^- presumably via the intermediacy of ClO_3^- with the production of a water molecule at each step.[11] Despite a favorable reduction potential, perchlorate reductase does not further reduce ClO_2^-. Instead, chlorite is further reduced to environmentally benign chloride (Cl^-) and dioxygen (O_2) in a reaction catalyzed by chlorite dismutase (Cld), a heme-containing enzyme.[12] This enzyme is of considerable interest since photosystem II is the only other known enzymatically catalyzed process for O−O bond formation. Dubois and co-workers have studied the mechanism of Cld and proposed that the resting Fe^{III}-heme reacts with ClO_2^- to form compound I and ClO^-, which quickly rebounds to give O_2 and Cl^-.[13] Our group has also reported on the disproportionation of chlorite mainly to chloride and chlorate

Received: January 7, 2014
Published: February 5, 2014

   dx.doi.org/10.1021/ja5001642 | J. Am. Chem. Soc. 2014, 136, 3680−3686

under physiological pH using water-soluble iron porphyrins as catalysts.[14]

Unlike their iron analogues, manganese porphyrin complexes have been shown, independently, by us and the Groves group to catalyze chlorine dioxide formation from chlorite.[15,16] Lau and co-workers have reported on a ruthenium bisphenanthroline complex that produces ClO_2.[17] Industrially, there are several methods for the production of chlorine dioxide. Nonetheless, chlorine oxyanions (ClO_n^-) are the prevalent source of ClO_2 in every method. The majority of methods, however, involve highly corrosive conditions and harsh oxidants, which raise health and environmental/safety concerns.[18] Of the chlorine oxyanions used for ClO_2 production, ClO_3^- is the most common source via the reaction with methanol in the presence of concentrated sulfuric acid.[19] However, the one-electron electrochemical oxidation of chlorite offers an alternative route to ClO_2 but requires a substantial input of energy. The primary commercial use of chlorine dioxide is as an oxidizing agent for pulp bleaching and more recently for water disinfection/treatment.[19] Chlorine dioxide is preferred over chlorine gas (Cl_2) for water treatment as it exhibits superior antimicrobial activity and generates less harmful byproducts (chlorinated species or trihalomethanes).[20] One major drawback is the instability of ClO_2 at high pressure, a fact that effectively prohibits its transport as a gas. Hence, on-site production of ClO_2 is a prerequisite for any practical application.

Our group communicated on the high reactivity of non-heme manganese−oxo complexes, $[Mn^{IV}(O)(Bn\text{-}TPEN)]^{2+}$ (Bn-TPEN = *N*-benzyl-*N*,*N*′,*N*′-tris(2-pyridylmethyl)-1,2-diaminoethane) and $[Mn^{IV}(O)(N4Py)]^{2+}$ (N4Py = *N*,*N*-bis(2-pyridylmethyl)bis(2-pyridyl)methylamine) (see Figure 1), in

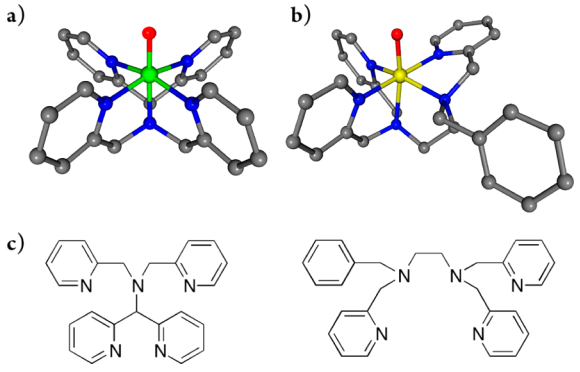

Figure 1. DFT-optimized structures of the catalysts used in the conversion of chlorite to chlorine dioxide: (a) $[Mn^{IV}(O)(N4Py)]^{2+}$, (b) $[Mn^{IV}(O)(Bn\text{-}TPEN)]^{2+}$, and (c) N4Py (left) and Bn-TPEN (right).

oxidation reactions.[21] Herein, we provide a catalytic process for the generation of chlorine dioxide from chlorite using two non-heme manganese(II) complexes, $[Mn^{II}(N4Py)]^{2+}$ and $[Mn^{II}(Bn\text{-}TPEN)]^{2+}$. The reaction proceeds efficiently reaching completion within 30 min with as little as 0.10 mol % catalyst loading under ambient temperature and noncorrosive pH. The catalytic formation of chlorine dioxide is observed for both $[Mn^{II}(N4Py)]^{2+}$ and $[Mn^{II}(Bn\text{-}TPEN)]^{2+}$ with second-order rate constants of 21 and 6 M^{-1} s^{-1}, respectively. For the non-heme manganese complexes in this report, catalysis initiates via OAT (oxygen atom transfer) to generate a putative $Mn^{IV}(O)$ species. As chlorine dioxide is produced, a $Mn^{III}(OH)$ species accumulates and the ClO_2 product acts as an inhibitor of the reaction. A comprehensive mechanism that satisfies all experimental observations is obtained from quantitative kinetics modeling.

RESULTS

Formation of ClO_2. The catalytic activity of $[Mn^{II}(N4Py)]^{2+}$ and $[Mn^{II}(Bn\text{-}TPEN)]^{2+}$ for ClO_2 production from ClO_2^- was examined at 25.0 °C in 50.0 mM acetate buffer at pH 5.00. Strikingly, if the pH of the buffer is increased then the production of ClO_2 is halted with the disproportionation of chlorite to chloride and chlorate instead being favored. This observation suggests the process for ClO_2 production is proton dependent. Additionally, when the buffer composition is changed from acetate to citrate, the production of ClO_2 is halted suggesting that the buffer is not innocent during catalysis. The formation of ClO_2 was monitored following its characteristic absorption band at λ_{max} = 360 nm (ε = 1250 M^{-1} cm^{-1}). The ClO_2 product can be extracted from the aqueous medium into diethyl ether. A typical spectrum of extracted ClO_2 from the catalytic reaction is shown in Figure 2a and is

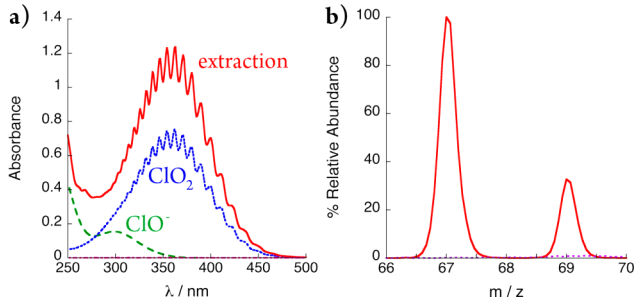

Figure 2. UV−vis spectroscopy and ESI-MS evidence for the formation of chlorine dioxide gas during catalysis. (a) UV−vis spectra of an authentic sample of ClO_2 in diethyl ether (dotted blue), an extraction of ClO_2 from the catalytic reaction (solid red), difference spectrum/hypochlorite (dashed green), chlorite spectrum (dotted pink). (b) ESI-MS of extracted ClO_2 from catalysis, using 10.0 μM $[Mn^{II}(N4Py)]^{2+}$ and 8.00 mM ClO_2^- (solid red) and chlorite (dashed pink) in diethyl ether.

compared to an authentic sample of ClO_2. Negative mode electrospray ionization mass spectroscopy (ESI-MS) of the diethyl ether extract confirmed that ClO_2 (*m*/*z* 67.0) and ClO_3^- (*m*/*z* 83.0) were formed during the reaction. Chlorite is insoluble in diethyl ether, hence the peak at 67.0 *m*/*z* is that of ClO_2 and not ClO_2^- (Figure 2b). Dioxygen (O_2) was not observed in any of the reactions performed.

Products Analysis by Ion Chromatography (IC). Ion chromatography was used to identify and quantify chlorine-containing anionic products. IC was performed on reaction mixtures upon maximum yield/concentration of ClO_2, confirming that the majority of the chlorite reactant was consumed and both Cl^- and ClO_3^- were also formed. When the concentration of chlorite or catalyst was increased, more chlorate was formed. Longer reaction times led to the complete decomposition of chlorite, while the concentration of chlorine dioxide remained relatively constant. The exact yields of anions of selected reaction conditions are summarized in Table 1. Ion chromatograms and exact yields of anions for all reactions are provided in the Supporting Information (Figures S2−S24 and Tables S1−S5).

dx.doi.org/10.1021/ja5001642 | J. Am. Chem. Soc. 2014, 136, 3680−3686

Table 1. Results for the Catalytic Conversion of Chlorite to Chlorine Dioxide in 50.0 mM Acetate Buffer (pH 5.00)[a]

catalyst	[cat]/ μM	$[ClO_2^-]_0$	$[ClO_2^-]_f$	$[Cl^-]$	$[ClO_3^-]$	$[ClO_2]$	% ClO_2[b]	% ox. equiv.[c]
Mn(N4Py)	10.0	10.0	4.24	2.24	1.79	1.68	29	22
Mn(N4Py)	10.0	4.00	1.10	1.10	0.88	0.91	31	20
Mn(N4Py)	100[d]	4.00	0.32	1.39	1.62	0.64	17	16
Mn(Bn-TPEN)	50.0	10.0	3.67	2.83	1.63	1.82	29	34
Mn(Bn-TPEN)	50.0	4.00	0.95	1.35	0.71	0.96	31	34
Mn(Bn-TPEN)	109[d]	4.00	0.86	1.49	0.64	1.01	35	39
Mn(N4Py)	10.0			0.01	0.12	0.61 − 0.47[e]		
Mn(Bn-TPEN)	50.0			0.07	0.35	0.47 − 0.04[e]		

[a]All concentrations are mM unless otherwise stated. Chlorine dioxide concentrations were quantified by using UV−vis spectroscopy on the reaction mixture. Ion chromatography was used to quantify the concentrations of other chlorine-containing species. Ion chromatograms were performed at 1 h unless otherwise stated. [b]Percentage calculated by using the final concentration of chlorine dioxide divided by the concentration of reacted chlorite. [c]Percentage of oxidizing equivalence unaccounted for by chlorine-containing species. [d]Ion chromatogram taken at maximum ClO_2 formation. [e]Chlorine dioxide prepared separately in acetate buffer. The range represents $[ClO_2]_0$ and 20 min after injection of catalyst.

Reactivity of Chlorine Dioxide with Manganese(II) and Manganese(III) Complexes. To test how the product affects the reaction, ClO_2 was collected in acetate buffer (pH 5.00) from a separate reaction and the reactivity of both catalysts with ClO_2 was examined. The reaction of ClO_2 with precatalyst, manganese(II) species, resulted in a rapid decrease in the absorption band for ClO_2 and the appearance of a $Mn^{III}(OH)$ species for both manganese complexes.[21] $[Mn^{II}(N4Py)]^{2+}$ was more reactive toward ClO_2 in comparison to $[Mn^{II}(Bn\text{-}TPEN)]^{2+}$ as shown in Figure 3. The reaction of

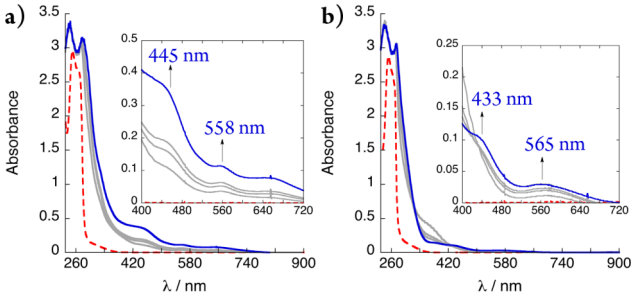

Figure 3. Examination of product inhibition by reacting ClO_2 with the manganese catalysts, $[Mn^{II}(N4Py)]^{2+}$ and $[Mn^{II}(Bn\text{-}TPEN)]^{2+}$. The dashed red spectrum is the starting catalyst. UV−vis scans at 2, 7, 12, 180, and 360 s. (a) The reaction of $[Mn^{II}(N4Py)]^{2+}$ (500 μM) and chlorine dioxide (1.15 mM) results in the rapid disappearance of ClO_2 and the appearance of a $Mn^{III}(OH)$ species (see inset). (b) The reaction of $[Mn^{II}(Bn\text{-}TPEN)]^{2+}$ (500 μM) and chlorine dioxide (1.15 mM) results in a slower disappearance of ClO_2 and the appearance of a $Mn^{III}(OH)$ species (see inset).

ClO_2 with the resting state form of the catalyst, manganese(III) species, resulted in a slower decrease in absorption for ClO_2 relative to starting with $Mn^{II}(OH_2)$ (Figures S25 and S26, Supporting Information). This observation implies that the decomposition of ClO_2 is dependent on the oxidation state of the catalyst.

Absorption Spectroscopy and Kinetics. The consumption of chlorite can be monitored by the decrease in absorbance at 260 nm (ε = 154 M^{-1} cm^{-1}); however, both catalysts have a maximum absorption at this wavelength. Furthermore, the absorption of the catalyst increases as $Mn^{III}(OH)$ accumulates over the course of the reaction. Therefore, the reaction kinetics were studied following the formation of ClO_2 at 360 nm albeit the $Mn^{III}(OH)$ form of the catalyst also absorbs in this region but with minimal contribution due to its low extinction coefficient. While the time profiles at 360 nm (ClO_2) fit a single exponential equation to a first approximation, the time profiles exhibit features of more complex kinetics (see Figures 4 and 5).

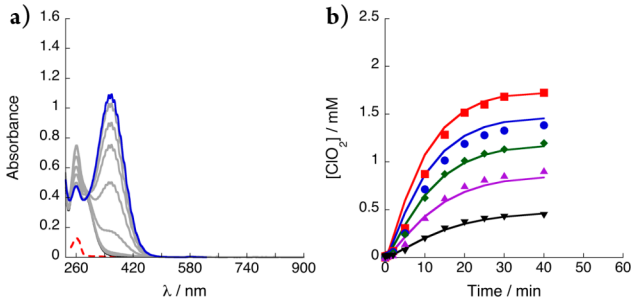

Figure 4. Kinetics of ClO_2 formation with use of $[Mn^{II}(N4Py)]^{2+}$ as a catalyst. (a) UV−vis spectral changes of the reaction over 40 min. Initial catalyst (dashed), first and last scan (solid), others gray. Conditions: $[Mn^{II}(N4Py)]$ = 10.0 μM; $[ClO_2^-]$ = 4.05 mM. (b) Changes in concentration of ClO_2 versus time. Solid lines represent kinetic modeling fits. Conditions: $[Mn^{II}(N4Py)]_0$ = 10.0 μM; $[ClO_2^-]_0$ = 9.85, 7.37, 6.00, 4.14, 1.95 mM (top to bottom).

Ion chromatography confirms that the majority of the chlorite is consumed (except for starting with high chlorite concentration of 10.0 mM) when the maximum concentration of ClO_2 is reached.

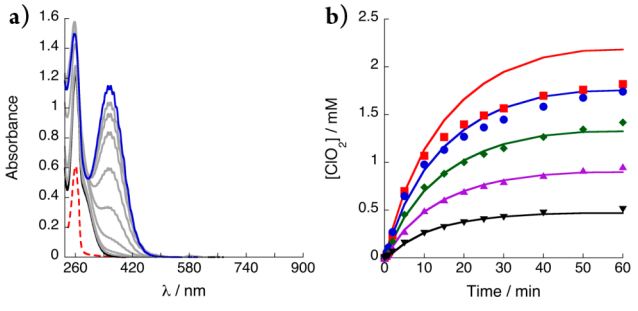

Figure 5. Kinetics of ClO_2 formation with use of $[Mn^{II}(Bn\text{-}TPEN)]^{2+}$ as a catalyst. (a) UV−vis spectral changes of the reaction for 1 h. Initial catalyst (dashed), first and last scan (solid), others gray. Conditions: $[Mn^{II}(Bn\text{-}TPEN)]$ = 50.0 μM; $[ClO_2^-]$ = 4.00 mM. (b) Change in concentration of ClO_2 versus time. Solid lines represent kinetic modeling fits. Conditions: $[Mn^{II}(Bn\text{-}TPEN)]_0$ = 50.0 μM; $[ClO_2^-]_0$ = 9.99, 7.93, 5.99, 4.02, 2.09 mM (top to bottom).

dx.doi.org/10.1021/ja5001642 | J. Am. Chem. Soc. 2014, 136, 3680−3686

The kinetics for $[Mn^{II}(N4Py)]^{2+}$ and $[Mn^{II}(Bn\text{-}TPEN)]^{2+}$ were examined. When a solution of chlorite (2.00−10.0 mM) was monitored in the presence of $[Mn^{II}(N4Py)]^{2+}$ (10.0 μM), an induction period was observed before the appearance of ClO_2. This induction period ranged from 5 to 300 s, depending on the initial catalyst concentration. When a solution of chlorite (2.00−10.0 mM) was monitored in the presence of $[Mn^{II}(Bn\text{-}TPEN)]^{2+}$ (50.0 μM), an induction period was not observed and ClO_2 followed approximately first-order kinetics. A 5-fold increase in the concentration of $[Mn^{II}(Bn\text{-}TPEN)]^{2+}$ was necessary to achieve comparable reaction times as a result of its lower reactivity (Figures 4b and 5b).

Preliminary inspection of the data shows dependence on $[ClO_2^-]$ and [Mn]. While the rate of reaction increases linearly with respect to [Mn] (Figures S11a and S21a, Supporting Information), the dependence on $[ClO_2^-]$, the limiting reagent, is more complex (Figures S11b and S21b, Supporting Information). Furthermore, the amount of ClO_2 produced is dependent on $[ClO_2^-]$ in a nonlinear fashion (Table 1) with a maximum yield of ca. 31%. The sensitivity of ClO_2 yield indicates product inhibition or further decomposition of ClO_2 at high concentrations. It should also be noted that even with $[ClO_2^-]_0$ = 10.0 mM, ClO_2 production plateaus at ca. 1.82 mM. The effect of the product on the catalyst's state was investigated by performing successive additions of chlorite, which is described next.

Multiple Additions of ClO_2^-. The reactivity of both catalysts upon multiple additions of chlorite was examined. ClO_2^- (4.00 mM) was reacted with $[Mn^{II}(N4Py)]^{2+}$ (10.0 μM) or $[Mn^{II}(Bn\text{-}TPEN)]^{2+}$ (50.0 μM). Upon reaching the maximum concentration of ClO_2, the mixture was purged with argon gas for 5 min to remove the ClO_2 product. A second aliquot of ClO_2^- (4.00 mM) was added to the catalyst solution and the kinetics of ClO_2 formation was monitored. A decrease in the observed rate was observed for both catalysts, $[Mn^{II}(N4Py)]^{2+}$ with a 40% decrease while $[Mn^{II}(Bn\text{-}TPEN)]^{2+}$ had a 66% decrease, as a result of catalyst deactivation (Figure 6).

Time-Dependent Product Distribution. To further elucidate the mechanism for chlorine dioxide formation, the concentrations of all chlorine-containing species were analyzed at 10-min intervals by ion chromatography (ClO_2^-, Cl^-, ClO_3^-) and UV−vis spectroscopy (ClO_2) and fit by kinetic modeling. As expected, the reaction products chloride, chlorate, and chlorine dioxide are produced as chlorite is consumed (Figure 7). Chlorine dioxide reaches a plateau within 30 min while the concentration of both chloride and chlorate continues to increase over time.

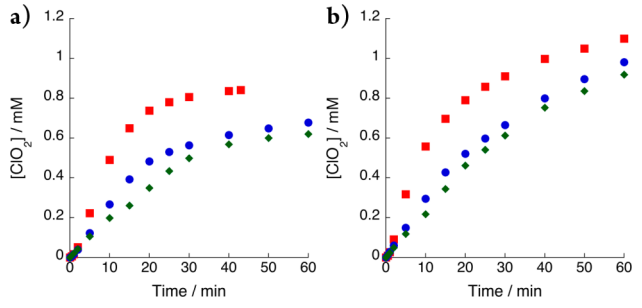

Figure 6. Further conversion to ClO_2 upon multiple additions of chlorite to the manganese catalysts $[Mn^{II}(N4Py)]^{2+}$ and $[Mn^{II}(Bn\text{-}TPEN)]^{2+}$. Concentration of ClO_2 versus time for multiple additions of $[ClO_2^-]$ = 4.00 mM upon purging the reaction mixture of ClO_2. First addition (squares), second addition (circles), third addition (diamonds). (a) $[Mn^{II}(N4Py)]$ = 10.0 μM; (b) $[Mn^{II}(Bn\text{-}TPEN)]$ = 50.0 μM.

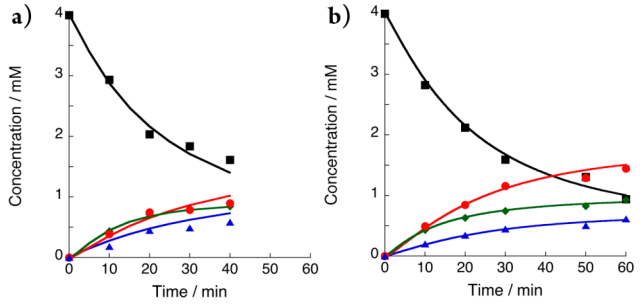

Figure 7. Time-dependent concentrations of chlorine-containing species during catalysis. ClO_2^- (squares), Cl^- (diamonds), ClO_3^- (circles), and ClO_2 (triangles). Solid lines represent kinetic modeling fits. (a) Reaction with use of $[Mn^{II}(N4Py)]^{2+}$ as catalyst. Conditions: $[Mn^{II}(N4Py)]$ = 10.0 μM; $[ClO_2^-]_0$ = 4.00 mM. (b) Reaction with use of $[Mn^{II}(Bn\text{-}TPEN)]^{2+}$ as catalyst. Conditions: $[Mn^{II}(Bn\text{-}TPEN)]$ = 50.0 μM; $[ClO_2^-]_0$ = 4.00 mM.

Electron Paramagnetic Resonance (EPR). EPR spectroscopy was used to identify the change in oxidation state of the manganese catalysts. Both ClO_2^- (4.00 mM) and ClO_2 (1.00 mM) were reacted independently with $[Mn^{II}(N4Py)]^{2+}$ (500 μM) and $[Mn^{II}(Bn\text{-}TPEN)]^{2+}$ (500 μM) in acetate buffer (pH 5.00). Figure 8 shows the EPR spectra for $[Mn^{II}(N4Py)]^{2+}$ and its reaction with ClO_2^- and ClO_2. The reactions with chlorite were allowed to continue for 1 h, purged of ClO_2 with use of argon, and frozen. The same procedure was carried out for the reactions with ClO_2, except the reaction time was only 20 min. In these reactions, the characteristic signal for Mn^{II} is not observed and a feature that can be assigned to a $Mn^{III}(\mu\text{-}O)Mn^{IV}$ dinuclear complex emerges.[22] Both catalysts gave identical EPR spectra under reaction conditions. The EPR spectra for $[Mn^{II}(Bn\text{-}TPEN)]^{2+}$ can be found in the Supporting Information (Figure S1). Mn^{III} (S = 2) and Mn^{V} (S = 1 or 0) would not be observable in perpendicular mode EPR.

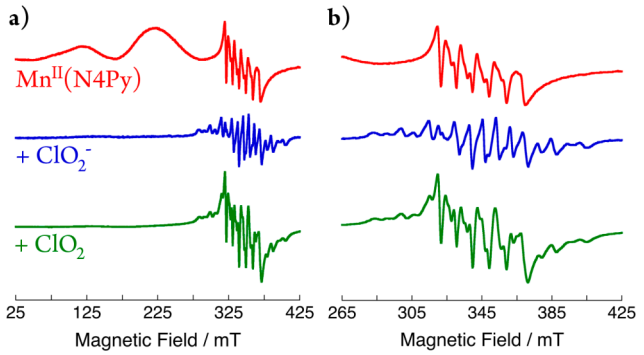

Figure 8. (a) Formation of a $Mn^{III}(\mu\text{-}O)Mn^{IV}$ dinuclear species confirmed by EPR spectroscopy when the manganese catalyst $[Mn^{II}(N4Py)]^{2+}$ is reacted with chlorite and chlorine dioxide. Conditions: $[Mn^{II}(N4Py)]$ = 500 μM reacted with $[ClO_2^-]$ = 4.00 mM or $[ClO_2]$ = 1.15 mM. (b) Expanded region of signals assigned to a $Mn^{III}(\mu\text{-}O)Mn^{IV}$ dinuclear species.

dx.doi.org/10.1021/ja5001642 | J. Am. Chem. Soc. 2014, 136, 3680−3686

DISCUSSION

Catalytic oxidation of ClO_2^- to ClO_2 by two water-soluble non-heme manganese complexes has been studied at 25.0 °C and pH 5.00. To our knowledge, this is the first example of manganese non-heme complexes that catalyze this conversion. Good yields of ClO_2 were observed in less than 1 h with use of as little as 0.10 mol % $[Mn^{II}(N4Py)]^{2+}$ and 0.50 mol % $[Mn^{II}(Bn\text{-}TPEN)]^{2+}$. These catalyst loadings correspond to turnover frequencies (TOF), defined as $[ClO_2]$ produced per mole of catalyst loading per hour, of 1000 and 200 h^{-1}, respectively. Since the production of ClO_2 in situ and on-site is important for industrial applications, these non-heme manganese catalysts offer a convenient route to ClO_2 production under reasonably mild and noncorrosive conditions with use of an earth-abundant metal and readily available ligands.

Several manganese(III) porphyrin complexes have been examined for the catalytic formation of chlorine dioxide independently by our group and that of Groves.[15,16] The initial step for the heme complexes is oxygen atom transfer from chlorite to $[Mn^{III}]$ via either heterolytic or homolytic Cl−O bond cleavage of chlorite. Homolytic Cl−O bond cleavage results in a $Mn^{IV}(O)$ complex while heterolytic cleavage results in a $Mn^{V}(O)$ cationic species. A proposed mechanism for the catalytic conversion of ClO_2^- to ClO_2 for manganese porphyrin catalysts is given in Scheme 1.

Scheme 1. General Mechanism for the Conversion of ClO_2^- to ClO_2 with Use of Water-Soluble Manganese Porphyrin Catalysts

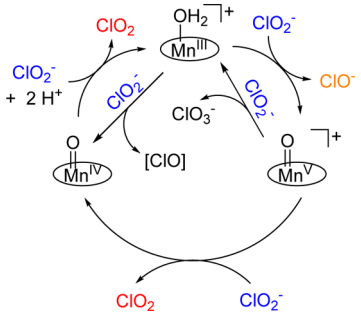

In contrast to the previously described manganese porphyrin systems, our non-heme catalysts described herein are present in the +2 oxidation state and are 5-coordinate. Over the course of the reaction, the $Mn^{II}(OH_2)$ species is fully consumed giving rise to higher oxidation states of the manganese complexes as evident by UV−vis (Figure 3) and EPR spectroscopy (Figure 8). The relatively low stability of the $Mn^{IV}(O)$ species supported by N4Py and Bn-TPEN ligation in water solution suggests that this species does not accumulate at sufficient concentrations to be detected. These observations are in contrast to manganese porphyrin complexes where the precatalyst, $[Mn^{III}]^+$, remains the dominant form of the catalyst with $Mn^{IV}(O)$ and $[Mn^{V}(O)]^+$ species being proposed intermediates in the catalytic cycle. Another stark difference is the observed induction period when using $[Mn^{II}(N4Py)]^{2+}$ as a catalyst. The induction period indicates slower formation of the active species in comparison to $[Mn^{II}(Bn\text{-}TPEN)]^{2+}$ as a result of lower catalyst loading. The dominant observable form of the catalyst under catalysis is a $Mn^{III}(OH)$ species (UV−vis 440 and 560 nm). This complex has been prepared independently for the Bn-TPEN ligand.[21] The $Mn^{IV}(O)$ is expected to exhibit an absorption band at higher wavelength (ca. 1040 nm); furthermore, $Mn^{III}(OH)$ is also responsible for the increase in absorption at 260 nm (Figure 3). These observations as well as proposed reaction steps (Scheme 2) were used to predict the concentrations of these manganese species over the course of the reaction by using a mathematical model as shown in Figure 9.

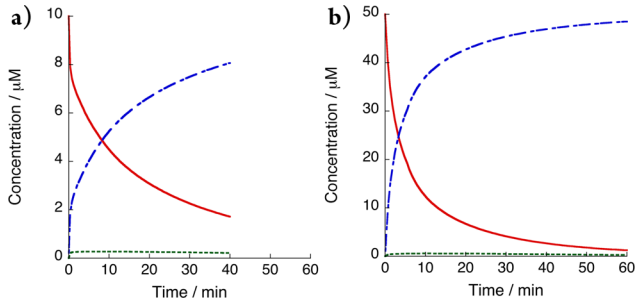

Figure 9. Predicted time-dependent concentrations of proposed manganese oxidation states versus reaction time. $Mn^{II}(OH_2)$ (solid red), $Mn^{III}(OH)$ (dashed blue), $Mn^{IV}(O)$ (dashed green). (a) With $[Mn^{II}(N4Py)]^{2+}$ as catalyst. Conditions: $[Mn^{II}(N4Py)]$ = 10.0 μM; $[ClO_2^-]$ = 4.00 mM. (b) With $[Mn^{II}(Bn\text{-}TPEN)]^{2+}$ as catalyst. Conditions: $[Mn^{II}(Bn\text{-}TPEN)]$ = 50.0 μM; $[ClO_2^-]$ = 4.00 mM.

Even though not observed directly, the putative $Mn^{IV}(O)$ and its participation is substantiated by the observation in the EPR spectra of a $Mn^{III}(\mu\text{-}O)Mn^{IV}$ dinuclear species.[22] The first-order dependence on [Mn] effectively rules out this dinuclear species as the active form of the catalyst, which would afford second-order kinetic dependence on catalyst. All of these observations are consistent with activation of the precatalyst via an OAT reaction with ClO_2^- forming $Mn^{IV}(O)$ and ClO^- (eq 1) to enter the proposed catalytic cycle in Scheme 2. The hypochlorite formed does not rebound with the newly formed manganese−oxo species to form dioxygen but instead quickly reacts with excess chlorite to form chloride and chlorine dioxide (eq 7) with reaction kinetics provided in Figure S43, Supporting Information. The high-valent manganese−oxo species then has three fates: (1) react via a PCET reaction with chlorite to give ClO_2 and $Mn^{III}(OH)$ (eq 2), (2) react via an OAT reaction with chlorite to form chlorate and precatalyst (eq 3), or (3) reacting with the dominant form of the catalyst, $Mn^{III}(OH)$, to form the dinuclear $Mn^{III}(\mu\text{-}O)Mn^{IV}$ species. The first pathway produces chlorine dioxide, which involves protonation of the oxo ligand on Mn^{IV} and hence accounts for the observed pH dependence for ClO_2 production. The second pathway results in the formation of chlorate and precatalyst, which quickly reacts with chlorine dioxide (eq 4) to form $Mn^{III}(OH)$ thus re-entering the catalytic cycle. The chlorate that is formed does not react with either of the catalysts under the conditions used. The dominant species, $Mn^{III}(OH)$, reacts with chlorite in the presence of protons via homolytic Cl−O bond cleavage to form [ClO] and regenerate the $Mn^{IV}(O)$ species (eq 5). This proposal has precedence in the iron heme systems based on DFT calculations.[23] The [ClO] radical byproduct is known to react with chlorite to make ClO^- and ClO_2.[24] [ClO] also reacts with ClO_2 to give $[Cl_2O_3]$, which disproportionates in water to HOCl, ClO_3^-, and H^+.[25] However, in our proposed reaction mechanism the [ClO] species reacts with the buffer (acetate) to form chloride and peracetic acid (eq 8). To account for the apparent slow

dx.doi.org/10.1021/ja5001642 | J. Am. Chem. Soc. 2014, 136, 3680−3686

Scheme 2. Proposed Mechanism for the Conversion of ClO_2^- to ClO_2 with Use of Two Water-Soluble Non-Heme Manganese Complexes

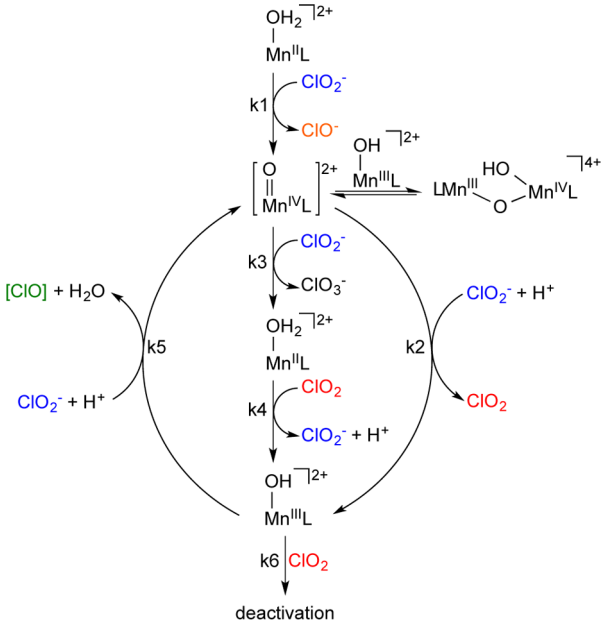

$$Mn^{II}(OH_2)L + ClO_2^- \xrightarrow{k_1} Mn^{IV}(O)L + ClO^- + H_2O \quad (1)$$

$$Mn^{IV}(O)L + ClO_2^- + H^+ \xrightarrow{k_2} Mn^{III}(OH)L + ClO_2 \quad (2)$$

$$Mn^{IV}(O)L + ClO_2^- + H_2O \xrightarrow{k_3} Mn^{II}(OH_2)L + ClO_3^- \quad (3)$$

$$Mn^{II}(OH_2)L + ClO_2 \xrightarrow{k_4} Mn^{III}(OH)L + ClO_2^- + H^+ \quad (4)$$

$$Mn^{III}(OH)L + ClO_2^- + H^+ \xrightarrow{k_5} Mn^{IV}(O)L + [ClO] + H_2O \quad (5)$$

$$Mn^{III}(OH)L + ClO_2 \xrightarrow{k_6} \text{deactivation} \quad (6)$$

$$2\,ClO_2^- + ClO^- + 2\,H^+ \xrightarrow{k_7} 2\,ClO_2 + Cl^- + H_2O \quad (7)$$

$$2\,[ClO] + 3\,C_2H_3O_2^- + H_3O^+ \xrightarrow{k_8} 2\,Cl^- + 3\,C_2H_4O_3 \quad (8)$$

down and eventual cessation of the production of ClO_2 as well as other species, the deactivation reaction assumed to be either ligand oxidation or metal dissociation is included (eq 6). Rate constants, obtained from mathematical modeling, for the reaction steps described are given in Table 2. The rate constant (k_8) for eq 8 is fast enough to be considered instantaneous relative to the other proposed reactions.

Table 2. Rate Constants for the Catalytic Conversion of Chlorite to Chlorine Dioxide in Acetate Buffer (pH 5.00)[a]

catalyst	k_1	k_2	k_3	k_4	k_5	k_6	k_7 ($M^{-2/3}$ s^{-1})[b]
Mn(N4Py)	19.2	207	500	74	21	0.29	0.18
Mn(Bn-TPEN)	2.9	265	173	33	6.3	0.45	0.18

[a]All rate constants are in M^{-1} s^{-1} unless otherwise stated. See Scheme 2, eqs 1–7, for reaction steps. [b]In eq 7, the reaction is 1st order in [ClO^-] and 2/3 order in [ClO_2^-]. Determination of reaction order is described in the Supporting Information.

The mathematical model accurately predicts the induction period observed for $[Mn^{II}(N4Py)]^{2+}$ where the reaction of precatalyst with chlorite is slow relative to subsequent reactions. An induction period was not observed for $[Mn^{II}(Bn\text{-}TPEN)]^{2+}$ as a result of higher catalyst loading. The model also predicts that the reactivity of chlorite with $Mn^{III}(OH)$ (k_5) is slower than that of $Mn^{IV}(O)$ (k_2) supporting the observation that $Mn^{III}(OH)$ is the dominant form during catalysis. The disappearance of the characteristic $Mn^{II}(OH_2)$ signal by EPR spectroscopy suggests that the precatalyst, if regenerated, is quickly converted to higher oxidation state species. According to the mathematical model the assumption that precatalyst is generated but quickly converted is validated by the observed product inhibition.

A word is in order here regarding the overall stoichiometry of the reaction. The precatalyst enters the catalytic cycle by converting chlorite to hypochlorite via OAT (eq 1), which then reacts with chlorite to produce 2:1 equivalence of ClO_2:Cl^- (eq 7). Subsequent formation of ClO_2 from chlorite is expected to produce 1:1 equivalence of ClO_2:Cl^- for the outer cycle shown in Scheme 2. The inner reaction pathway results in a 1:1 equivalence of ClO_3^-:Cl^-. The resulting balanced equation results in a 2:1:1 equivalence of Cl^-:ClO_2:ClO_3^-, which is consistent with the product ratios when using $[Mn^{II}(Bn\text{-}TPEN)]^{2+}$ as the catalyst. All balanced reactions can be found in the Supporting Information. Our product ratios in Table 1 show variable values that depend on the starting concentrations of chlorite. All of the converted chlorite can be accounted for by the three products ClO_2, Cl^-, and ClO_3^-. However, a significant oxidizing equivalent is not accounted for in the chlorine-containing products. For example, in the first entry of Table 1, 5.76 mM of ClO_2^- is converted. Based on Cl(III) oxidation state, this corresponds to a reactants overall oxidation state equivalent of +17.28. The products are 2.24 mM Cl^- (oxidation state equivalent of −2.24), 1.79 mM ClO_3^- (oxidation state equivalent of +8.95), and 1.68 mM ClO_2 (oxidations state equivalent of +6.72). While the total of products comes to 5.76 mM, accounting for nearly all the chlorite conversion, the net oxidation state equivalent of the products is +13.43, leaving ca. 22% of the reactants oxidizing equivalents not accounted for. We probed for potential water oxidation by looking to see if O_2 is produced. The result was negative, no O_2 was observed. That limits the possibilities to the oxidation of the buffer. This theory is supported by the halt in ClO_2 formation when the buffer composition was changed from acetate to citrate with the same buffer capacity and pH. However, we were unable to detect acetate oxidation products in our system by mass spectrometry. It is noted that acetate buffer is frequently used in studying kinetics of ClO_2 reactions.[25]

Multiple additions of ClO_2^- for both catalysts were conducted to determine whether the catalysts were still active for the catalytic formation of ClO_2. Both manganese catalysts remained active for the production of ClO_2; however, slower reaction rates were observed with relatively comparable yields of ClO_2. This can be attributed to the relatively robust nature of the ligands and their manganese complexes under oxidizing conditions allowing for the observed high turnover numbers (TON) for ClO_2 formation of 2160 and 560 for $[Mn^{II}(N4Py)]^{2+}$ and $[Mn^{II}(Bn\text{-}TPEN)]^{2+}$, respectively. These turnover numbers result from three successive additions of chlorite with a mild decrease in ClO_2 yield suggesting that even higher turnovers can be obtained.

CONCLUSIONS

Two non-heme coordination complexes of manganese, $[Mn^{II}(N4Py)]^{2+}$ and $[Mn^{II}(Bn\text{-}TPEN)]^{2+}$, catalyze the formation of chlorine dioxide from chlorite under ambient temperature at pH 5.00. The catalysts are robust and stable

dx.doi.org/10.1021/ja5001642 | J. Am. Chem. Soc. 2014, 136, 3680−3686

enough to afford 1000 turnovers per hour and still remain active in subsequent additions of chlorite. Kinetic and spectroscopic studies revealed that a $Mn^{III}(OH)$ species is the dominant form of the catalyst under reaction conditions. However, a $Mn^{III}(\mu\text{-}O)Mn^{IV}$ dinuclear species is observed by EPR spectroscopy, which supports the involvement of a putative $Mn^{IV}(O)$ species. The first-order kinetic dependence on the manganese catalyst precludes the $Mn^{III}(\mu\text{-}O)Mn^{IV}$ dinuclear species as the active form of the catalyst. Based on quantitative kinetic modeling, a mechanism has been put forth to explain the experimental observations (Scheme 2). The chlorine dioxide producing cycle involves formation of a $Mn^{IV}(O)$, which undergoes PCET reactions with chlorite to afford ClO_2. The proposed mechanism differs from that of the manganese porphyrin systems as a result of the difference in ligand coordination to the metal as well as the starting oxidation state. While the chlorine mass balance is excellent and the converted chlorite can be fully accounted for by the observed three products, ClO_2, Cl^-, and ClO_3^-, a significant oxidizing equivalent is not accounted for by the experimentally observed stoichiometric ratios of products. Nevertheless, the ClO_2 product can be efficiently removed from the aqueous reaction mixture via purging with an inert gas. These manganese non-heme catalysts offer a new method for the preparation of pure chlorine dioxide for on-site use, and further production of ClO_2. They also circumvent the need to use the higher molecular weight, more expensive, and more elaborate prophyrin ligand systems.

■ ASSOCIATED CONTENT

Supporting Information

The synthesis and characterization of $[Mn^{II}(N4Py)]^{2+}$ and $[Mn^{II}(Bn\text{-}TPEN)]^{2+}$ complexes; ion chromatograms for all of the reactions performed; EPR spectroscopy of $[Mn^{II}(Bn\text{-}TPEN)]^{2+}$ and the reactions with chlorite and chlorine dioxide; details on the proposed mechanism that include balanced reactions and other potential reactions; and predicted concentrations of the different oxidation states of manganese during catalysis based on mathematical modeling of the mechanism. This material is available free of charge via the Internet at http://pubs.acs.org.

■ AUTHOR INFORMATION

Corresponding Author

wwnam@ewha.ac.kr; mabuomar@purdue.edu

Notes

The authors declare no competing financial interest.

■ ACKNOWLEDGMENTS

This research has been supported by grants from the NSF (CHE-1110475 to M.M.A.-O.) and the KRF/MEST of Korea through CRI, GRL (2010-00353), and WCU (R31-2008-000-10010-0) (to W.N.).

■ REFERENCES

(1) (a) EPA (2002 External Review Draft) "Perchlorate environmental contamination: toxicological review and risk characterization" 2001, Washington, D.C. (b) Urbansky, E. T.; Schock, M. R. *J. Environ. Mangage.* **1999**, *56*, 79−95.

(2) Motzer, W. E. *Environ. Forensics* **2001**, *2*, 301−311.

(3) Coates, J. D.; Achenbach, L. A. *Perchlorate, Environmental Occurrence, Interactions and Treatment*; Eds.: Gu, B., Coates, J. D., Eds.; Springer: New York, NY, 2006; pp 279−291.

(4) Abu-Omar, M. M. *Chem. Commun.* **2003**, *17*, 2102−2111.

(5) (a) Deshwal, B. R.; Jo, H. D.; Lee, H. K. *Can. J. Chem. Eng.* **2004**, *82*, 619−623. (b) Jia, Z.; Margerum, D. W.; Francisco, J. S. *Inorg. Chem.* **2000**, *39*, 2614−2620. (c) Furman, C. S.; Margerum, D. W. *Inorg. Chem.* **1998**, *37*, 4321−4327. (d) Cosson, H.; Ernst, W. R. *Ind. Eng. Chem. Res.* **1994**, *33*, 1468−1475. (e) Leitner, N. K. V.; Delaat, J.; Dore, M. *Water Res.* **1992**, *26*, 1655−1664.

(6) Fábián, I. *Coord. Chem. Rev.* **2001**, *216−217*, 449−472.

(7) Collman, J. P.; Boulatov, R.; Sunderland, C. J.; Shiryaeva, I. M.; Berg, K. E. *J. Am. Chem. Soc.* **2002**, *124*, 10670−10671.

(8) Slaughter, L. M.; Collman, J. P.; Eberspacher, T. A.; Brauman, J. I. *Inorg. Chem.* **2004**, *43*, 5198−5204.

(9) EPA 816-F-03−016, June 2003; available for download at http://www.epa.gov/safewater/mcl.html.

(10) (a) Coates, J. D.; Achenbach, L. A. *Nat. Rev. Microbiol.* **2004**, *2*, 569−580. (b) Thorell, H. D.; Stenklo, T. K.; Karlsson, J.; Nilsson, T. *Appl. Environ. Microbiol.* **2003**, *69*, 5585−5592.

(11) (a) Giblin, T.; Frankenberger, W. T. *Microbiol. Res.* **2001**, *156*, 311−315. (b) Kengen, S. W. M.; Rikken, G. B.; Hagan, W. R.; van Ginkel, C. G.; Stams, A. J. M. *J. Bacteriol.* **1999**, *181*, 6706−6711. (c) Okeke, B. C.; Frankenberger, W. T. *Microbiol. Res.* **2003**, *158*, 337−344.

(12) (a) Hagedoorn, P. L.; de Geus, D. C.; Hagan, W. R. *Eur. J. Biochem.* **2002**, *269*, 4905−4911. (b) Thorell, H. D.; Karlsson, J.; Portelius, E.; Nilsson, T. *Biochim. Biophys. Acta* **2002**, *1577*, 445−451. (c) Stenklo, K.; Thorell, H. D.; Bergius, H.; Aasa, R.; Nilsson, T. *J. Biol. Inorg. Chem.* **2001**, *6*, 601−607. (d) Thorell, H. D.; Beyer, N. H.; Heegaard, N. H. H.; Ohman, M.; Nilsson, T. *Eur. J. Biochem.* **2004**, *271*, 3539−3546. (e) Xu, J. L.; Logan, B. E. *J. Microbiol. Methods* **2003**, *54*, 239−247. (f) O'Connor, S. M.; Coates, J. D. *Appl. Environ. Microbiol.* **2002**, *68*, 3108−3113.

(13) (a) Streit, B. R.; DuBois, J. L. *Biochemistry* **2008**, *47*, 5271−5280. (b) Lee, A. Q.; Streit, B. R.; Zdilla, M. J.; Abu-Omar, M. M.; DuBois, J. L. *Proc. Natl. Acad. Sci. U.S.A.* **2008**, *105*, 15654−15659.

(14) Zdilla, M. J.; Lee, A. Q.; Abu-Omar, M. M. *Inorg. Chem.* **2009**, *48*, 2260−2268.

(15) Hicks, S. D.; Petersen, J. L.; Bougher, C. J.; Abu-Omar, M. M. *Angew. Chem., Int. Ed.* **2011**, *50*, 699−702.

(16) (a) Umile, T. P.; Wang, D.; Groves, J. T. *Inorg. Chem.* **2011**, *50*, 10353−10362. (b) Umile, T. P.; Groves, J. T. *Angew. Chem., Int. Ed.* **2011**, *50*, 695−698.

(17) Hu, Z.; Du, H.; Man, W.-L.; Leung, C.-F.; Liang, H.; Lau, T.-C. *Chem. Commun.* **2012**, *48*, 1102−1104.

(18) Alternative Disinfectants and Oxidants, Guidance Manual (EPA 815-R-99−014), 1999; available at http://www.epa.gov/ogwdw/mdbp/pdf/alter/chapt_4.pdf.

(19) Vogt, H.; Balej, J.; Bennett, J. E.; Wintzer, P.; Sheikh, S. A.; Gallone, P.; Vasudevan, S.; Pelin, K. Chlorine Oxides and Chlorine Oxygen Acids. In *Ullmann's Encyclopedia of Industrial Chemistry*; Wiley-VCH: Weinheim, Germany, 2010; p 55.

(20) Ogata, N.; Shibata, T. *J. Gen. Virol.* **2008**, *89*, 60−67.

(21) (a) Wu, X.; Seo, M. S.; Davis, K. M.; Lee, Y.-M.; Chen, J.; Cho, K.-B.; Pushkar, Y. N.; Nam, W. *J. Am. Chem. Soc.* **2011**, *133*, 20088−20091. (b) Chen, J.; Lee, Y.-M.; Davis, K. M.; Wu, X.; Seo, M. S.; Cho, K.-B.; Yoon, H.; Park, Y. J.; Fukuzumi, S.; Pushkar, Y. N.; Nam, W. *J. Am. Chem. Soc.* **2013**, *135*, 6388−6391.

(22) (a) Huang, P.; Högblom, J.; Anderlund, M. F.; Sun, L.; Magnuson, A.; Styring, S. *J. Inorg. Biochem.* **2004**, *98*, 733−745. (b) Huang, P.; Magnuson, A.; Lomoth, R.; Abrahamsson, M.; Tamm, M.; Sun, L.; van Rotterdam, D.; Park, J.; Hammarstrom, L.; Akermark, B.; Styring, S. *J. Inorg. Biochem.* **2002**, *91*, 159−172.

(23) Keith, J. M.; Abu-Omar, M. M.; Hall, M. B. *Inorg. Chem.* **2011**, *50*, 7928−7930.

(24) Buxton, G. V.; Subhani, M. S. *J. Chem. Soc. Faraday Trans. 1* **1972**, *68*, 947−957.

(25) Cseko, G.; Horvath, A. K. *J. Phys. Chem. A* **2012**, *116*, 2911−2919.